



Anti-recombination organic dyes containing dendritic triphenylamine moieties for high open-circuit voltage of DSSCs



Hai Zhang^a, Jie Fan^b, Zafar Iqbal^a, Dai-Bin Kuang^{b,**}, Lingyun Wang^a, Derong Cao^{a,*}, Herbert Meier^c

^aSchool of Chemistry and Chemical Engineering, State Key Laboratory of Luminescent Materials and Devices, South China University of Technology, Guangzhou 510641, China

^bMOE Key Laboratory of Bioinorganic and Synthetic Chemistry, KLGEI of Environment and Energy Chemistry, School of Chemistry and Chemical Engineering, Sun Yat-sen University, Guangzhou 510275, China

^cInstitute of Organic Chemistry, University of Mainz, Mainz 55099, Germany

ARTICLE INFO

Article history:

Received 29 January 2013

Received in revised form

9 April 2013

Accepted 18 April 2013

Available online 28 April 2013

Keywords:

Dye-sensitized solar cell

Non-planar

Sensitizer

Triphenylamine

Recombination

Open-circuit voltage

ABSTRACT

Three novel sensitizers with dendritic triphenylamine moieties were synthesized and used for dye-sensitized solar cells (DSSCs). Their absorption spectra, electrochemical and photovoltaic properties were extensively investigated. All three DSSCs exhibit high open-circuit voltage over 0.8 V. The photovoltaic results indicate that the dendritic triphenylamine units improve the open-circuit voltage, which is attributed to the retardation of charge recombination, demonstrating that non-planar and larger molecules exert better blocking function. Under standard global AM 1.5 solar conditions, the best performance of the DSSCs exhibits a short-circuit current density of 10.35 mA cm⁻², an open-circuit voltage of 0.836 V and a fill factor of 0.68, corresponding to an overall conversion efficiency of 5.87%.

© 2013 Elsevier Ltd. All rights reserved.

1. Introduction

Since the pioneering work of O'Regan and Grätzel in 1991 [1], dye-sensitized solar cells (DSSCs) have received considerable attention due to their low-cost fabrication and high power conversion efficiency. Tremendous efforts have been made to improve the photovoltaic performance of DSSCs [2–19]. Recently, over 12%, 11% and 10% [18,20–22] conversion efficiencies have been achieved by employing zinc, ruthenium complex dyes and metal free organic dyes under air mass 1.5 global (AM 1.5 G) irradiation, respectively. Although organic dyes have advantages like high molar extinction co-efficients, easy to fabrication over Ru complex dyes, but organic dyes show lower efficiency than **N719**. For instance, compared with the open-circuit voltage (V_{oc}) of more than 0.8 V for **N719**, organic dyes show relatively lower V_{oc} ranging from 0.55 V to 0.75 V for

triphenylamine dyes, coumarin dyes, carbazole dyes, indoline dyes and fluorine dyes [11,23–35], which is mainly due to the excessive loss of voltage during the dye-regeneration reaction. The usage of iodide/triiodide electrolyte as a redox shuttle limits the attainable open-circuit voltage (V_{oc}), to 0.7–0.8 V and is thus a major drawback [20]. Therefore, in order to further improve the efficiency of DSSCs, it is urgent to reduce the charge recombination and increase the electron injection efficiency. Additionally, charge recombination and electron injection efficiency are closely correlated with V_{oc} , which means V_{oc} becomes one of the principle factors accounting for the further improvement of the performance of DSSCs [36–40]. Photovoltage is determined by the difference between conduction-band edge of TiO₂ and redox potential. The conduction-band energy can be modified by interfacial environment. Thus, photovoltage can be tuned by different dye attached on TiO₂ surface because of the interfacial modification [23]. In recent years, various efforts such as sensitizer modification, usage of additives, co-adsorbents, and novel redox couples have been made to improve V_{oc} [41–44].

Typically, triphenylamine unit is often used as an electron donor for the photosensitizers because of its aggregation resistant

* Corresponding author. Tel./fax: +86 20 87110245.

** Corresponding author. Tel.: +86 20 84113015.

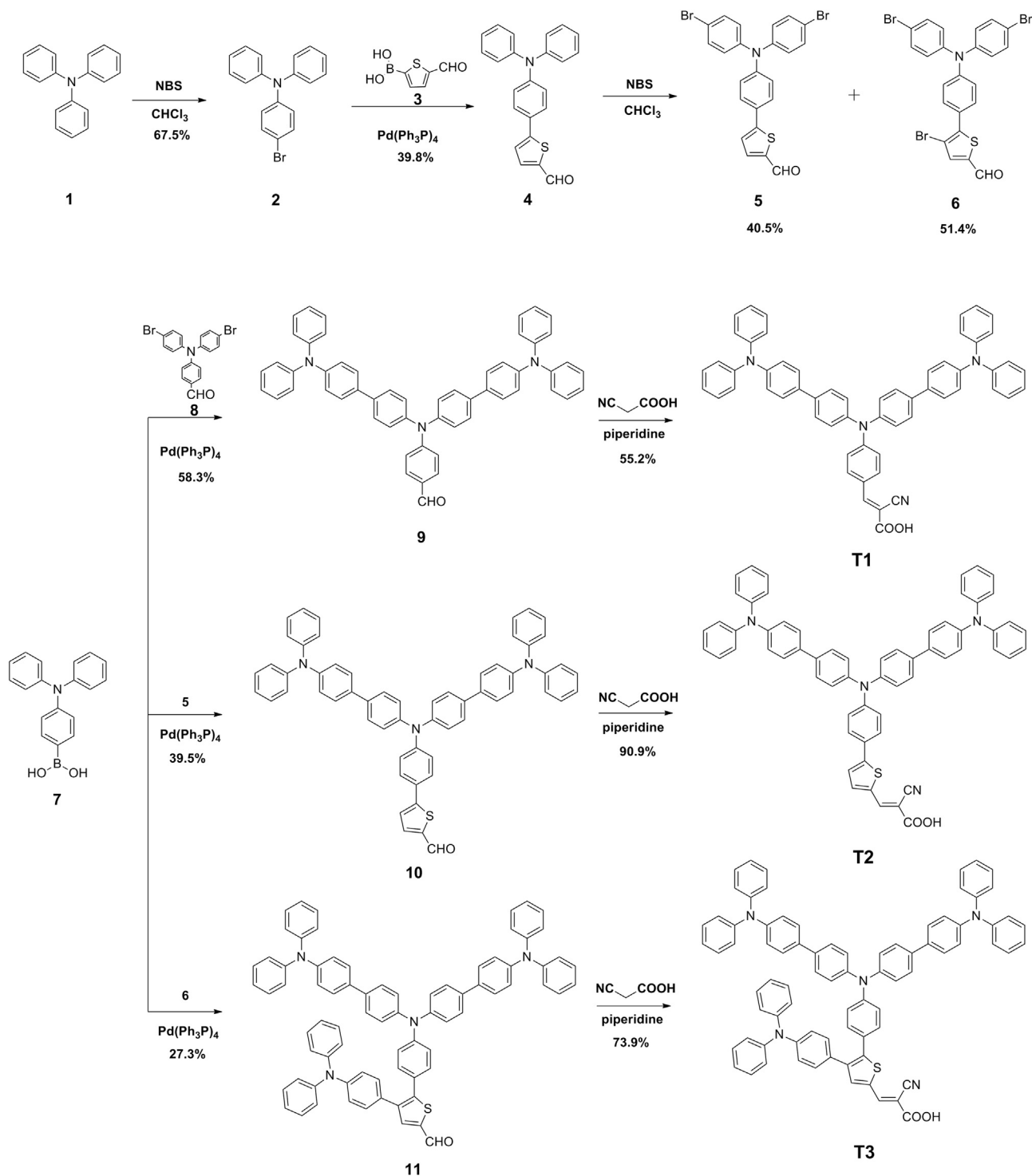
E-mail addresses: kuangdb@mail.sysu.edu.cn (D.-B. Kuang), drcao@scut.edu.cn (D. Cao).

non-planar molecular configuration as well as excellent electron donating capability [45,46]. Despite of a variety of molecular engineering of the TPA moiety, V_{oc} of TPA based dye has not been dramatically improved as expected over those of other organic dyes. Tian et al. reported that an extra arylamine group can stabilize the charge separated state and therefore enhance the value of V_{oc} [47,48]. Keeping in mind the above findings, we designed and synthesized three new organic dyes with dendritic triphenylamine moieties (**T1–3**) to enhance the open-circuit voltage of

DSSCs. Structural modifications were made to induce the bent conformation as well as steric hindrance (Scheme 1). Their absorption spectra, electrochemical, photovoltaic properties have been extensively investigated.

2. Experimental

All reagents were purchased from commercial sources and used without further purification unless otherwise noted. Solvents were



Scheme 1. Synthesis of the dyes **T1**, **T2** and **T3**.

freshly distilled from appropriate drying agents prior to use. Conventional Schlenk techniques were used, and reactions were carried out under argon or nitrogen. Reactions were monitored by using TLC and chromatographic separations were carried out on silica gel (300–400 mesh).

2.1. Synthesis

N,N-diphenyl-4-bromoaniline (**2**) [49], 5-[4-(diphenylamino)phenyl]thiophene-2-carbaldehyde (**4**) [49], 5-[4-[bis(4-bromophenyl)amino]phenyl]thiophene-2-carbaldehyde (**5**) [49], 4-[*N,N*-di(4-bromophenyl)amino]benzaldehyde (**8**) [50], 4-[bis(4-(diphenylamino)biphenyl-4-yl)amino]benzaldehyde (**9**) [50], were synthesized according to the methods reported in the literature with some modifications.

2.1.1. 5-[4-[Bis(4-bromophenyl)amino]phenyl]-4-bromothiophene-2-carbaldehyde (**6**)

Compound **4** (766 mg, 2.16 mmol) was dissolved in chloroform (50 mL) and the solution was cooled to 0 °C. *N*-bromosuccinimide (NBS) (2.3 g, 12.9 mmol) was added slowly and the mixture was stirred for 1 h at 0 °C. The mixture was allowed to warm to ambient temperature and stirring was continued for 4 h. Then the mixture was refluxed for 12 h. After being cooled to room temperature, the reaction mixture was extracted with dichloromethane (DCM). The combined organic layers were washed with water and brine, then dried over anhydrous MgSO₄. The solvent was removed via rotary evaporator, the residue was purified by column chromatography on silica gel (PE:DCM:EA = 30:15:1 as eluent) to give the product as a yellow solid in 51.4% (653 mg) yield, mp 170–172 °C. ¹H NMR (CDCl₃, 400 MHz): δ ppm 9.83 (s, 1H), 7.70 (s, 1H), 7.59 (m, 2H), 7.41 (m, 4H), 7.07 (m, 2H), 7.01 (m, 4H); ¹³C NMR (100 MHz, CDCl₃): δ ppm 181.5, 148.3, 147.8, 145.7, 140.6, 140.2, 132.7, 130.0, 126.6, 125.7, 122.3, 116.9, 108.1. APCI-MS: calculated for C₂₃H₁₅Br₃NOS (M+H)⁺/z 589.8419, found: 589.8282.

2.1.2. (*E*)-3-[4-[Bis(4'-(diphenylamino)-[1,1'-biphenyl]-4-yl)amino]phenyl]-2-cyanoacrylic acid (**T1**)

Compound **9** (300 mg, 0.395 mmol) was dissolved in 30 mL of chloroform, and cyanoacetic acid (67 mg, 0.788 mmol) was refluxed in the presence of piperidine (0.1 mL) for 20 h under argon. After cooling the reaction mixture was poured into water (30 mL) and extracted with DCM. The combined organic phases were dried over anhydrous MgSO₄, and the solvent was evaporated under reduced pressure. The pure product was obtained by column chromatography using silica gel (CH₂Cl₂:MeOH = 20:1 as eluent) as a red powder in 55.2% (180 mg) yield, mp 184–186 °C. ¹H NMR (DMSO-*d*₆, 400 MHz): δ ppm 7.81 (s, 1H), 7.94 (m, 2H), 7.68 (m, 4H), 7.60 (m, 4H), 7.35–7.31 (m, 8H), 7.26 (m, 4H), 7.09–6.99 (m, 18H); ¹³C NMR (100 MHz, DMSO-*d*₆): δ ppm 164.5, 151.7, 147.5, 147.2, 144.6, 137.0, 133.6, 133.2, 130.1, 128.1, 127.9, 126.8, 124.7, 123.8, 123.6, 119.7, 117.8, 100.0. HRMS-ESI: calculated for C₅₈H₄₂N₄O₂ (M)⁺/z 826.3302, found: 826.3311.

2.1.3. 5-[4-[Bis(4'-(diphenylamino)-[1,1'-biphenyl]-4-yl)amino]phenyl]thiophene-2-carbaldehyde (**10**)

A mixture of **5** (434 mg, 0.85 mmol), **7** (734 mg, 2.54 mmol), tetrakis(triphenylphosphine)palladium(0) (97 mg, 0.084 mmol), and potassium carbonate (3.3 mL of 2 M aqueous solution, 6.77 mmol) in THF (25 mL) was stirred and heated to reflux under argon for 20 h. The reaction mixture was poured into water and extracted with DCM, and the combined extracts were washed with brine, dried over anhydrous MgSO₄. The solvent was removed by rotary evaporation, and the crude product was purified by column chromatography on silica gel to give the product as a yellow solid.

Yield: 281 mg, 39.5%. mp 144–146 °C. ¹H NMR (CDCl₃, 400 MHz): δ ppm 9.85 (s, 1H), 7.70 (d, *J* = 4 Hz, 1H), 7.56–7.54 (m, 2H), 7.51–7.49 (m, 4H), 7.47–7.45 (m, 4H), 7.31 (d, *J* = 4 Hz, 1H), 7.28–7.24 (m, 7H), 7.21–7.19 (m, 4H), 7.16–7.12 (m, 14H), 7.04–7.01 (m, 5H); ¹³C NMR (100 MHz, CDCl₃): δ ppm 182.3, 165.5, 154.5, 148.9, 147.1, 145.7, 144.3, 141.4, 137.7, 136.1, 134.4, 129.3, 127.6, 127.4, 127.3, 126.5, 125.3, 124.4, 124.0, 123.0, 122.8. HRMS-ESI: calculated for C₅₉H₄₃N₃OS (M+H)⁺/z 841.3121, found: 841.3128.

2.1.4. (*E*)-3-[5-[4-(Bis(4'-(diphenylamino)-[1,1'-biphenyl]-4-yl)amino)phenyl]thiophen-2-yl]-2-cyanoacrylic acid (**T2**)

A solution of compound **10** (163 mg, 0.194 mmol) in chloroform (30 mL) and cyanoacetic acid (33 mg, 0.387 mmol) was refluxed in the presence of piperidine (0.03 mL) for 20 h under Argon. After cooling, the solution was poured into water (30 mL) and the mixture was extracted with DCM. The combined organic phases were dried over anhydrous MgSO₄, and evaporated under reduced pressure. The pure product was obtained by silica gel chromatography (CH₂Cl₂:MeOH = 20:1 as eluent) as a red powder in 90.9% (160 mg) yield, mp 208–209 °C. ¹H NMR (DMSO-*d*₆, 400 MHz): δ ppm 8.28 (s, 1H), 7.82 (s, 1H), 7.64–7.62 (m, 2H), 7.56–7.50 (m, 8H), 7.30–7.27 (m, 8H), 7.10–6.97 (m, 23H); ¹³C NMR (100 MHz, CDCl₃): δ ppm 147.6, 146.9, 145.4, 135.8, 134.2, 134.1, 129.2, 129.0, 128.2, 127.5, 127.3, 125.4, 125.2, 124.4, 124.2, 123.9, 123.8, 122.9, 122.8. HRMS-ESI: calculated for C₆₂H₄₄N₄O₂S (M)⁺/z 908.3179, found: 908.2934.

2.1.5. 5-[4-[Bis(4'-(diphenylamino)-[1,1'-biphenyl]-4-yl)amino]phenyl]-4-(4-(diphenylamino)phen-yl)thiophene-2-carbaldehyde (**11**)

A mixture of **6** (633 mg, 1.07 mmol), **7** (1.24 g, 4.29 mmol), tetrakis(triphenylphosphine)palladium(0) (148 mg, 0.128 mmol), and potassium carbonate (6 mL of 2 M aqueous solution, 12.8 mmol) in THF (50 mL) was stirred and heated to reflux under argon for 20 h. The reaction mixture was poured into water (50 mL) and extracted with DCM. The combined extract was washed with brine and dried over anhydrous MgSO₄. The solvent was removed by rotary evaporation, and the crude product was purified by column chromatography on silica gel to give the product as a yellow solid in 27.3% (317 mg) yield, mp 155–157 °C. ¹H NMR (CDCl₃, 400 MHz): δ ppm 9.88 (s, 1H), 7.75 (s, 1H), 7.50–7.45 (m, 8H), 7.28–7.10 (m, 35H), 7.05–7.01 (m, 11H); ¹³C NMR (100 MHz, CDCl₃): δ ppm 182.7, 148.5, 148.2, 147.7, 147.3, 147.0, 145.8, 140.4, 139.4, 138.6, 136.0, 134.4, 129.9, 129.7, 129.6, 129.3, 129.0, 127.6, 127.4, 125.2, 124.7, 124.4, 124.0, 123.2, 122.9, 122.1. HRMS-ESI: calculated for C₇₇H₅₆N₄O₂S (M)⁺/z 1084.4169, found: 1084.4014.

2.1.6. (*E*)-3-[5-[4-(Bis(4'-(diphenylamino)-[1,1'-biphenyl]-4-yl)amino)phenyl]-4-(4-(diphenylamino)phen-yl)thiophen-2-yl]-2-cyanoacrylic acid (**T3**)

A solution of compound **11** (300 mg, 0.276 mmol), cyanoacetic acid (47 mg, 0.553 mmol) in chloroform (30 mL) was refluxed in the presence of piperidine (0.04 mL) for 20 h under Argon. After cooling, the reaction mixture was poured into water (30 mL) and extracted with DCM. The combined organic phase was dried over anhydrous MgSO₄, and evaporated under reduced pressure. The pure product was obtained by silica gel column chromatography (CH₂Cl₂:MeOH = 20:1 as eluent) as a red powder in 73.9% (235 mg) yield, mp 193–195 °C. ¹H NMR (DMSO-*d*₆, 400 MHz): δ ppm 8.32 (s, 1H), 7.90 (s, 1H), 7.54–7.50 (m, 8H), 7.31–7.15 (m, 16H), 7.09–6.88 (m, 30H); ¹³C NMR (100 MHz, CDCl₃): δ ppm 147.7, 147.4, 147.3, 147.0, 145.6, 136.1, 134.3, 130.0, 129.9, 129.7, 129.3, 127.6, 127.4, 125.4, 125.3, 124.7, 124.6, 124.4, 124.0, 123.2, 122.9, 122.8, 121.9. HRMS-ESI: calculated for C₈₀H₅₇N₅O₂S (M)⁺/z 1151.4227, found: 1151.4065.

2.2. Measurement

^1H and ^{13}C NMR spectra were recorded on a Bruker 400 MHz spectrometer in CDCl_3 or $\text{DMSO}-d_6$ with tetramethylsilane as inner reference. The melting point was taken on Tektronix X4 microscopic melting point apparatus and uncorrected. The absorption and emission spectra of the dyes in chloroform solution (1×10^{-5} M) were measured at room temperature by Shimadzu UV-2450 UV-Vis spectrophotometer and Fluorolog III photoluminescence spectrometer, respectively. The absorption spectra of the dyes on TiO_2 film were measured by UV-3010 UV-Vis spectrophotometer. Electrochemical redox potentials were measured by Cyclic Voltammetry (CV), using three electrode cells and an Ingsens 1030 electrochemical workstation (Ingsens Instrument Guangzhou, Co. Ltd., China) in a one compartment at a scan rate of 50 mV/s. The Ag/AgCl in KCl (3 M) solution and an auxiliary platinum wire were utilized as reference and counter electrodes while dye coated TiO_2 films were used as working electrode. Tetrabutylammonium perchlorate ($n\text{-Bu}_4\text{NClO}_4$) 0.1 M in THF was used as supporting electrolyte. All electrochemical measurements were calibrated by using ferrocene as standard (0.63 V vs. NHE). The current voltage characteristics were recorded by using a Keithley 2400 source meter under simulated AM 1.5 G ($100 \text{ mW}/\text{cm}^2$) illumination with a solar light simulator (Oriel, Model: 91192). A 1000 W Xenon arc lamp (Oriel, Model:6271) served as a light source and its incident light intensity was calibrated with an NREL standard Si solar cell. The incident monochromatic photon-to-current conversion efficiency (IPCE) spectra were measured as a function of wavelength from 350 to 800 nm on the basis of a Spectral Products DK240 monochromator. The electrochemical impedance spectra (EIS) measurements were conducted on the electrochemical workstation (Zahner Zennium) in dark condition, with an applied bias potential of -0.84 V. A 10 mV AC sinusoidal signal was employed over the constant bias with the frequency ranging between 1 MHz and 10 mHz. The impedance parameters were determined by fitting of the impedance spectra using Z-view software. The amount of dye load was measured by desorbing the dye from the films with 0.1 M NaOH in THF/ H_2O (1:1) and measuring UV-Vis spectrum.

2.3. Fabrication of DSSCs

Fluorine-doped tin oxide (FTO) glasses were washed with detergent, water, ethanol and acetone in an ultrasonic bath for removing dirt and debris. Anatase TiO_2 nano-particles (20 nm) were prepared through a hydrothermal treatment with a precursor solution containing $\text{Ti}(\text{O}i\text{Bu})_4$ (10 mL), ethanol (20 mL), acetic acid (18 mL) and deionized water (50 mL) according to the previously reported paper [51,52]. The synthesized TiO_2 powder (1.0 g) was ground for 40 min in the mixture of ethanol (8.0 mL), acetic acid

(0.2 mL), terpineol (3.0 g) and ethyl cellulose (0.5 g) to form homogeneous slurry. Finally, the slurry was sonicated for 15 min in an ultrasonic bath to form a viscous white TiO_2 paste. Then the TiO_2 photoanodes (about 16 μm in thickness) were prepared via screen-printing process onto FTO glass. The prepared films were annealed through a procedure (325°C for 5 min, 375°C for 5 min, 450°C for 15 min, and 500°C for 15 min) to remove the organic substances. Then TiO_2 films were soaked in 0.04 M TiCl_4 aqueous solution for 30 min at 70°C to improve the photocurrent and photovoltaic performance. Treated films were rinsed with deionized water and ethanol and then sintered again at 520°C for 30 min. After cooling to 80°C the films were immersed in a 5.0×10^{-4} M solution of **T1–3** dyes for 16 h (0.5 mM dye in dichloromethane). Afterward these films were rinsed with CH_2Cl_2 in order to remove physical adsorbed organic dye molecules. To evaluate their photovoltaic performance, the dye-sensitized TiO_2/FTO glass films were assembled into a sandwiched type together with Pt/FTO counter electrode. Platinized counter electrodes were fabricated by thermal depositing H_2PtCl_6 solution (5 mM in isopropanol) onto FTO glass at 400°C for 15 min. The electrolyte (0.6 M 1-methyl-3-propylimidazoliumiodide (PMII), 0.05 M LiI, 0.10 M guanidinium thiocyanate, 0.03 M I_2 and 0.5 M tert-butylpyridine) in acetonitrile/valeronitrile (85:15) was injected from a hole made on the counter electrode into the space between the sandwiched cells. The active area of the dye coated TiO_2 film was 0.16 cm^2 .

3. Result and discussion

3.1. Synthesis

The synthetic routes of three dyes are shown in Scheme 1. Intermediate **4** was prepared from TPA via bromination of compound **1** and Suzuki coupling reaction of compound **3**. Compounds **5** and **6** were obtained by bromination reaction of **4** using *N*-bromosuccinimide followed by the Michaelis–Arbuzov reaction. The Suzuki coupling reaction was made with the respective bromides and (4-(diphenylamino)phenyl)boronic acid (**7**) to yield the aldehydes **9**, **10** and **11**. Then, compound **9** was transformed into **T1** via Knoevenagel reaction in 55.2% yield. Similarly, compounds **T2** and **T3** were obtained in 90.9% and 73.9% yields, respectively. All the intermediates and target products were purified by column chromatography and the new compounds were characterized with standard spectroscopic techniques like ^1H NMR, ^{13}C NMR and HRMS.

3.2. Optical properties

Absorption and emission spectra of three dyes in dilute solutions of chloroform (1×10^{-5} M) are shown in Fig. 1a. The characteristic data are listed in Table 1. In the UV-Vis spectra, the dyes

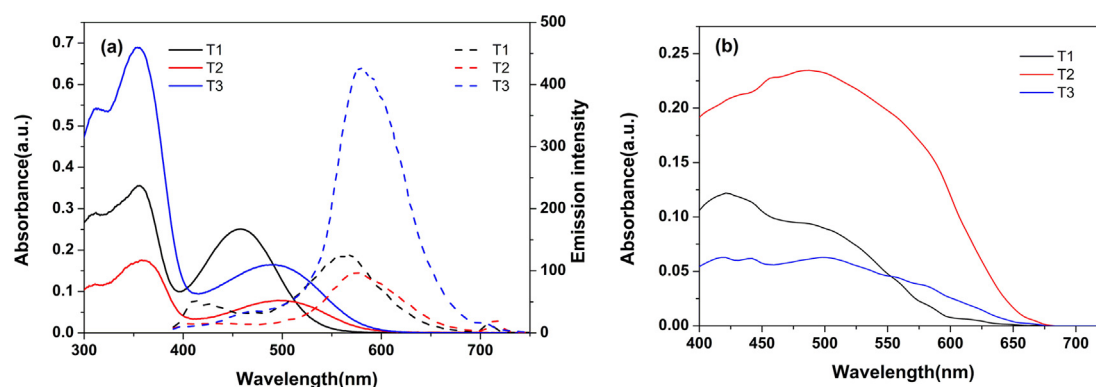


Fig. 1. Absorption and emission spectra of **T1–3** in CHCl_3 solutions (a) and on TiO_2 films (16 μm) (b).

Table 1
Band gap (calculated by DFT/B3LYP), absorption, and electrochemical parameters for organic dyes.

Dye	(HOMO/LUMO) ^a /eV	Band gap ^a	(λ_{abs}^b /nm)/(ϵ /M ⁻¹ cm ⁻¹)	λ_{abs} on TiO ₂ /nm	HOMO/eV ^c	E_{0-0} /eV ^d	LUMO/eV ^e
T1	-4.93/-2.25	2.68	356(35579), 458(25096)	421	-5.07	2.36	-2.71
T2	-4.83/-2.53	2.3	359(18661), 502(8363)	488	-5.12	2.25	-2.87
T3	-4.79/-2.47	2.32	354(68980), 493(16470)	498	-5.16	2.28	-2.88

^a DFT/B3LYP calculated values.

^b Absorptions of charge-transfer transition were measured in CHCl₃.

^c HOMO (vs. NHE) of dyes measured by cyclic voltammetry in 0.1 M tetrabutylammonium perchlorate in THF solution as supporting electrolyte, Ag/AgCl as reference electrode and Pt as counter electrode.

^d E_{0-0} : 0–0 transition energy measured at the onset of absorption spectra.

^e LUMO (vs. NHE) was calculated by HOMO– E_{0-0} .

exhibit two prominent bands, appearing at 300–400 nm and 400–600 nm, respectively. The former is ascribed to a localized aromatic π – π^* transition and the latter is of intramolecular charge-transfer character [53]. The intensity of π – π^* transitions was higher than that of the ICT (Fig. 1a). The absorption maxima for **T1**–**T3** in CHCl₃ are 458 nm, 502 nm and 493 nm in the visible region, respectively. Compounds **T2** and **T3** have thiophene group in conjugated chains, which enhance the extent of electron delocalization over the whole molecules, so their maximum absorption peaks are red shifted as compared to **T1**. The threshold wavelengths of the absorption spectra for **T1**, **T2** and **T3** are 551 nm, 583 nm, 595 nm, respectively, indicating that the introduction of a thiophene unit into the molecular structure of the sensitizers expanded and broadened the absorption range [53]. It is well known that a wider absorption range is favorable for the enhancement of the DSSCs performance, as more photons can be harvested. Under similar conditions the **T3** sensitizer shows an absorption peak at 493 nm that is slightly blue-shifted relative to that of **T2** which can be readily interpreted by the molecular modeling study of the two dyes. The ground state structure of **T3** possesses at 36.45° twist between B4 and S2 unit. The dihedral angle of S2 and B5 unit in **T3** is 47.57° (Fig. 2). For **T2**, the dihedral angles of the corresponding units are 20.46°, giving a more planar configuration. Accordingly, a red shift of **T2** compared to **T3** derives from more delocalization over an entire conjugated system in **T2**. Emission maxima of the dyes can be found at 500–700 nm when the dyes are excited at their respective absorption bands at 400–600 nm.

The absorption spectra of **T1**–**T3** on 16 μm TiO₂ films after 16 h absorption were measured (Fig. 1b). Compared to the spectrum in solution, the maximum absorption peaks of **T1** and **T2** on TiO₂ films were blue-shifted by 37 nm and 14 nm, respectively, which is possibly due to the deprotonation of carboxylic acid of the dye upon adsorption on the TiO₂ film or due to formation of H-aggregates [54,55]. However, the maximum absorption peak of **T3** was red-shifted by 5 nm (Table 1), which is possibly due to formation of J-aggregates of **T3** on the TiO₂ film [56].

3.3. Electrochemical properties

The oxidation potential (E_{ox}), corresponding to the highest occupied molecular orbital (HOMO) level of dyes, were measured by cyclic voltammetry (CV) in THF solutions on a dye films as working electrode (Fig. 3). As shown in Fig. 3 and Table 1, the ionization energy decreased gradually in the order of **T3** > **T2** > **T1**. It is noteworthy that inserting a thiophene unit close to the acceptor group promotes the HOMO level. Suitable HOMO and LUMO levels are necessary to match the conduction band (–0.5 V vs. NHE) of the TiO₂ electrode and the redox potential (0.4 V vs. NHE) of the iodine/iodide electrolyte. The excitation transition energies (E_{0-0}) were estimated to be 2.36 eV, 2.25 eV and 2.28 eV, respectively from the intersection of absorption and photoluminescence spectra. The HOMO and LUMO values vs. vacuum were transformed via the equation $E_{\text{HOMO}} = -e(4.88 + V_{\text{ox}})$ [18], where V_{ox} is the onset potential vs. ferrocene of reduction or oxidation of sensitizers. The energy offsets of LUMOs (–2.71 eV for **T1**, –2.87 eV for **T2** and –2.88 eV for **T3**) of dye molecules with respect to the titania conduction band edge (–4.00 eV) provide thermodynamic driving forces for charge generation. The energy offsets of HOMOs (–5.07 eV for **T1**, –5.12 eV for **T2** and –5.16 eV for **T3**) relative to that (–4.60 eV) of iodide supply negative Gibbs free energy changes for dye regeneration reaction. Through a systematic comparison on electrochemical data (Table 1) of all organic dyes, it is clear that the **T2** dye has a relative small HOMO/LUMO gap of 2.28 eV, generally consistent with its low-energy absorption peak.

3.4. Molecular orbital calculations

To get further insight into the geometrical and electronic distribution of the dyes, density functional theory (DFT) calculations were performed at B3LYP/6–31G* level with the Gaussian 03W program package. Energies and the electronic distribution of the frontier molecular orbitals (HOMOs and LUMOs) of the dyes **T1**–**T3** computed are presented in Fig. 4. In the optimized structures of

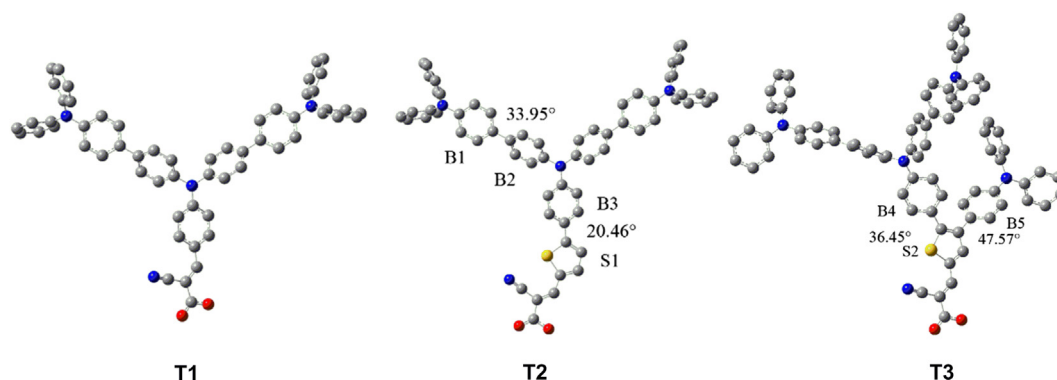


Fig. 2. The optimized geometries of the **T1**, **T2** and **T3** calculated with DFT on the B3LYP/6–31G* level.

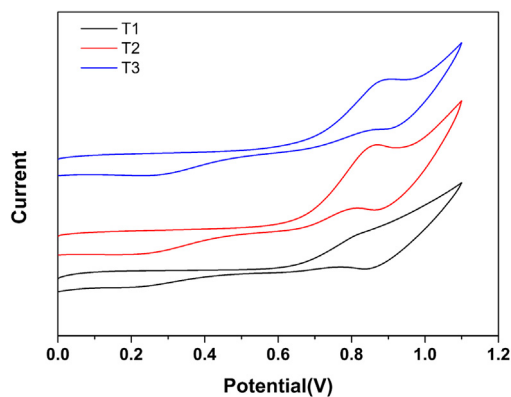


Fig. 3. Cyclic voltammogram plots of **T1–3** attached to nanocrystalline TiO_2 film deposited on conducting FTO glass.

three dyes, the electron cloud of the highest occupied frontier molecular orbitals were delocalized over the triphenylamine entities, while the lowest unoccupied molecular orbitals were mainly distributed over the cyanoacrylic acid groups. It suggests that HOMO to LUMO excitation moves the electron density distribution from triphenylamine donor moieties to cyanoacrylic acid acceptor moiety via different π -spacers. The effective intramolecular charge transfer process indicates that the electron injection from the excited dyes to titanium oxide CB is feasible. On the basis of these results, introduction of triphenylamine group into dye molecules is expected to give larger steric interactions, which would lead to less dye-aggregation on the TiO_2 thin film, resulting in enhanced DSSCs device performances.

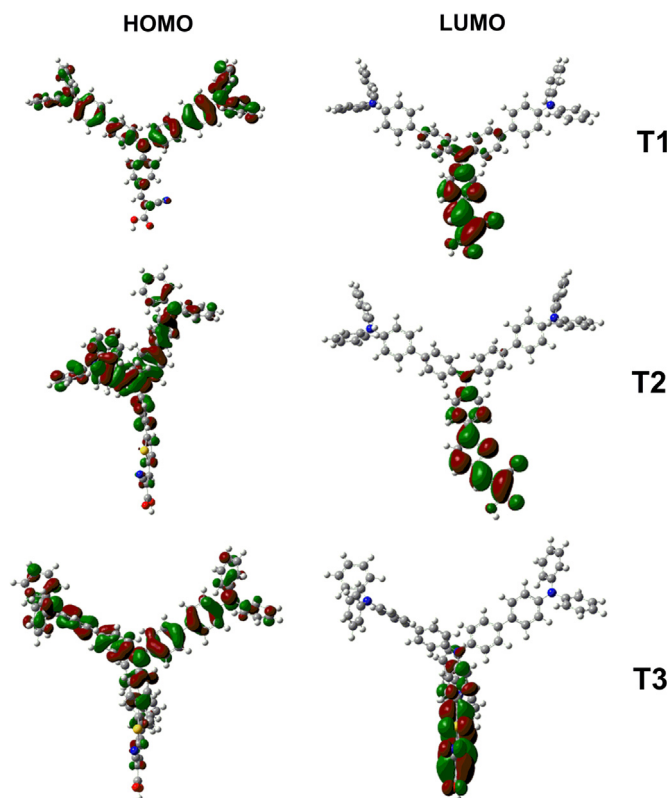


Fig. 4. The frontier orbitals of **T1**, **T2** and **T3** optimized at the B3LYP/6–31G* level.

3.5. Photovoltaic performances of the DSSCs

The incident monochromatic photon-to-current conversion efficiency as a function of incident wavelength for DSSCs based on the dyes using liquid electrolyte are shown in Fig. 5a. It is evident that all three dyes can efficiently convert visible light to photocurrent in the region from 400 nm to 700 nm. The IPCE of dye **T3** exceeds 70% over the spectral region from 420 nm to 530 nm, reaching its maximum of 78.1% at 470 nm and tail off toward 700 nm. J – V characteristics were further measured under irradiation of AM 1.5 G full sunlight and presented in Fig. 5b. It is noteworthy that all of the three dyes have high open-circuit voltages (853, 822 and 836 mV), which is due to the introduction of dendritic triarylamine antennas into the molecule to form the D–D– π –A structure. These structural modifications avoid the charge recombination processes of injected electrons with triiodide in the electrolyte and lead to an increase in open-circuit voltage [36,48]. **T2** dye based DSSCs showed a lower V_{oc} (822 mV) than **T1** and **T3** dyes based DSSCs. One plausible explanation is that the extended conjugation and good planarity can enhance the charge recombination and result in a lower V_{oc} [11,57]. As shown in Table 2, the **T3** dye-sensitized solar cell exhibits the best overall light-to-electricity conversion efficiency (η) of 5.87% with J_{sc} of 10.35 mA cm^{-2} , V_{oc} of 0.836 V, and a fill factor (ff) of 0.68. Under the similar conditions, the **T1** and **T2** dye-sensitized solar cell gave a J_{sc} value of 8.71 and 10.74 mA cm^{-2} , V_{oc} of 0.853 and 0.822 V and ff of 0.67 and 0.63, corresponding to an η value of 4.97% and 5.56%. From these results (Table 2), it was observed that the η value of **T2** based cell was higher than that of **T1** based cell due to a large J_{sc} . The poor efficiency of **T1** dye-sensitized cell was attributed to the lower light harvesting capability in visible range, evidenced by the UV–Vis absorption spectra (Fig. 1). A reverse trend was observed in J_{sc} , i.e. **T2** > **T3**, corresponding to 10.74 mA cm^{-2} , 10.35 mA cm^{-2} , respectively, for which the main reason may be too large a dihedral angle between the thiophene moiety (S2) and the benzene ring (B4), resulting in less efficient intramolecular charge transfer [58]. The adsorbed amounts on the TiO_2 films were measured as 1.28×10^{-7} , 1.51×10^{-7} , and $1.59 \times 10^{-7} \text{ mol cm}^{-2}$ for **T1**, **T2** and **T3**, respectively (Table 2).

When we nearly finished the experimental works, a series of similar dendritic triphenylamine dyes **TT1–3** were reported by Lu et al. [24]. The dendritic triphenylamine units were linked with vinyl group in the dyes. The **TT1–3** based DSSCs exhibited good performance, but their V_{oc} were not very high (0.65–0.71 V). A reasonable explanation is that the linker of vinyl group can keep more planar structure, and therefore reduce the bent conformation of the molecules. In our dyes the dendritic triphenylamine units were linked each other directly, inducing more bent conformation and leading to a higher V_{oc} (0.82–0.85 V).

Electrochemical impedance spectroscopy (EIS) analysis was performed to elucidate the photovoltaic findings (Fig. 6). Impedance spectra for **T1**, **T2** and **T3** dyes sensitized solar cells were measured in the dark condition under a forward bias of -0.84 V with a frequency range of 0.1 Hz–100 kHz. The Nyquist plots (Fig. 6) showed two semicircles, the small and large semicircles, respectively located in the high and middle frequency regions, which were assigned to charge transfer at Pt/electrolyte and TiO_2 /dye/electrolyte interface, respectively [11,59–62]. Small circles were almost similar in all the dyes due to the use of same counter electrode and electrolyte. Fig. 6 showed that the radius of the large semicircle were increased in the order of **T2** < **T3** < **T1**, indicating that the electron recombination resistance augments from **T2**, **T3** to **T1**. The electron

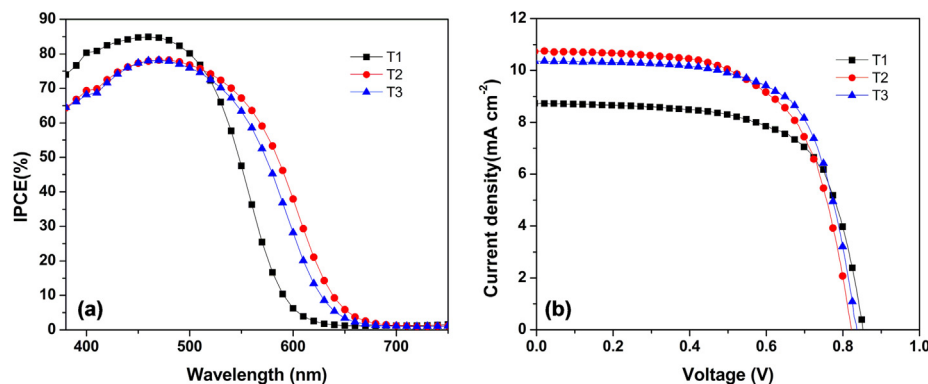


Fig. 5. (a) IPCE plots for the DSSCs. (b) J - V curves of DSSCs based on the dyes.

lifetime calculated by fitting the equation $\tau_r = R_{\text{rec}} \times \text{CPE2}$ (CPE2, chemical capacitance) [7,63,64] were 299 ms, 215 ms and 249 ms for **T1**, **T2** and **T3** dyes sensitized cells, respectively. The longer electron lifetime observed with **T1** dye-sensitized cells indicates more effective suppression of the recombination of the injected electron with the Γ^-/I_3^- in the electrolyte, leading to improvement in the V_{oc} . The result was also in agreement with the observed shift in the V_{oc} value under standard global AM 1.5 illumination. The dye **T2** has low electron lifetime as compared to the dye **T3**, indicating that the triphenylamine of the substituent at 4-position of thiophene may avoid the charge recombination, which leads to an increase in open-circuit voltage.

Table 2
Photovoltaic parameters for DSSCs of organic dyes.^a

Dye	$J_{\text{sc}}/\text{mA cm}^{-2}$	V_{oc}/mV	ff	H (%) ^b	τ/s ^c	Amount of dye load (mol cm^{-2})
T1	8.71	853	0.669	4.97	0.2993	1.28×10^{-7}
T2	10.74	822	0.630	5.56	0.2150	1.51×10^{-7}
T3	10.35	836	0.678	5.87	0.2492	1.59×10^{-7}

^a J_{sc} : short-circuit photocurrent density; V_{oc} : open-circuit photovoltage; ff : fill factor; η : total power conversion efficiency.

^b Performance of DSSCs measured in a 0.16 cm^2 working area on a FTO ($7 \Omega \text{ square}^{-1}$) substrate.

^c The electron lifetime calculated by fitting the equation $\tau_r = R_{\text{rec}} \times \text{CPE2}$ (CPE2, chemical capacitance).

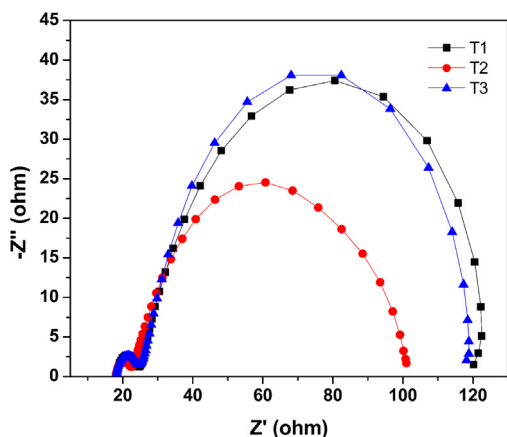


Fig. 6. Electrochemical impedance spectra measured in the dark for the DSSCs sensitized by **T1**, **T2** and **T3**, respectively.

4. Conclusion

In summary, three new dendritic triphenylamine-based D-D- π -A sensitizers (**T1**, **T2** and **T3**) were synthesized for DSSCs. The overall light-to-electricity conversion efficiency of the DSSCs sensitized with branched **T1**, **T2**, and **T3** dyes were 4.97%, 5.56%, and 5.87% respectively. As a result, compared to the reported organic dyes, high open-circuit voltages were obtained. Dye **T1** sensitized solar cell delivered the highest open-circuit photovoltage of 853 mV, which is related to introducing non-planar TPA moiety and thereby increasing steric hindrance against electron back reactions. By introducing the thiophene unit as π -bridge, V_{oc} obviously decreased. However, the open-circuit voltage increased significantly from 822 to 836 mV with the introduction of a TPA side chain at 4-position of thiophene. The results of this work indicate that the extended conjugation and good planarity can enhance the charge recombination and result in a lower V_{oc} , introducing bulky groups into side chain of π -bridge may be the effective method for increasing the open-circuit voltage of DSSCs.

Acknowledgments

We are grateful to the National Natural Science Foundation of China (21272079, 20873183, 21072064), the Natural Science Foundation of Guangdong Province, China (10351064101000000, S2012010010634) and the Fund from Guangzhou Science and Technology Project, China (2012J4100003) for the financial support.

References

- [1] O'Regan B, Grätzel M. A low-cost, high-efficiency solar cell based on dye-sensitized colloidal titanium dioxide films. *Nature* 1991;353(6346):737–40.
- [2] Nazeeruddin MK, Kay A, Rodicio L, Humphry-Baker R, Muller E, Liska P, et al. Conversion of light to electricity by cis-X₂Bis(2,2'-bipyridyl)-4,4'-dicarboxylate)ruthenium(II) charge-transfer sensitizers (X = Cl⁻, Br⁻, I⁻, CN⁻, and SCN⁻) on nanocrystalline TiO₂ electrodes. *J Am Chem Soc* 1993;115:6382–90.
- [3] Chiba Y, Islam A, Watanabe Y, Komiya R, Koide N, Han L. Dye-sensitized solar cells with conversion efficiency of 11.1%. *Jpn J Appl Phys* 2006;45:L638–40.
- [4] Hagberg D, Edvinsson T, Marinado T, Boschloo G, Hagfeldt A, Sun L. A novel organic chromophore for dye-sensitized nanostructured solar cells. *Chem Commun* 2006;2245–7.
- [5] Koumura N, Wang Z, Mori S, Miyashita M, Suzuki E, Hara K. Alkyl-functionalized organic dyes for efficient molecular photovoltaics. *J Am Chem Soc* 2006;128:14256.
- [6] Ito S, Zakeeruddin SM, Humphry-Baker R, Liska P, Charvet R, Comte P, et al. High-efficiency organic-dye-sensitized solar cells controlled by nanocrystalline-TiO₂ electrode thickness. *Adv Mater* 2006;18:1202–5.
- [7] Liao JY, Lei BX, Chen HY, Kuang DB, Su CY. Oriented hierarchical single crystalline anatase TiO₂ nanowire arrays on Ti-foil substrate for efficient flexible dye-sensitized solar cells. *Energy Environ Sci* 2012;5:5750–7.
- [8] Chen HY, Kuang DB, Su CY. Hierarchically micro-/nano-structured photoanode materials for dye-sensitized solar cells. *J Mater Chem* 2012;22(31):15475–89.

- [9] Liao JY, Lei BX, Kuang DB, Su CY. Tri-functional hierarchical TiO₂ spheres consisting of anatase nanorods and nanoparticles for high efficiency dye-sensitized solar cells. *Energy Environ Sci* 2011;4:4079–85.
- [10] Hwang S, Lee JH, Park C, Lee H, Kim C, Lee M-H, et al. A highly efficient organic sensitizer for dye-sensitized solar cells. *Chem Commun* 2007:4887–9.
- [11] Wang Z-S, Koumura N, Cui Y, Takahashi M, Sekiguchi H, Mori A, et al. Hexylthiophene-functionalized carbazole dyes for efficient molecular photovoltaics: tuning of solar-cell performance by structural modification. *Chem Mater* 2008;20(12):3993–4003.
- [12] Cao Y, Bai Y, Yu Q, Cheng Y, Liu S, Shi D, et al. Dye-sensitized solar cells with a high absorptivity ruthenium sensitizer featuring a 2-(hexylthio)thiophene conjugated bipyridine. *J Phys Chem C* 2009;113(15):6290–7.
- [13] Choi H, Baik C, Kang SO, Ko J, Kang M-S, Nazeeruddin MK, et al. Highly efficient and thermally stable organic sensitizers for solvent-free dye-sensitized solar cells. *Angew Chem Int Ed Engl* 2008;47(2):327–30.
- [14] Chen C, Wang M, Li J, Pootrakulchote N, Alibabaei L, Ngoc-le C, et al. Highly efficient light-harvesting ruthenium sensitizer for thin-film dye-sensitized solar cells. *ACS Nano* 2009;3(10):3103–9.
- [15] Grätzel M. Recent advances in sensitized mesoscopic solar cells. *Acc Chem Res* 2009;42(11):1788–98.
- [16] Li D, Qin D, Deng M, Luo Y, Meng Q. Optimization the solid-state electrolytes for dye-sensitized solar cells. *Energy Environ Sci* 2009;2:283–91.
- [17] Koumura N, Wang Z, Miyashita M, Sekiguchi H, Cui Y, Mori A, et al. Substituted carbazole dyes for efficient molecular photovoltaics: long electron lifetime and high open circuit voltage performance. *J Mater Chem* 2009;19:4829–36.
- [18] Zeng W, Cao Y, Bai Y, Shi Y, Zhang M, Wang F, et al. Efficient dye-sensitized solar cells with an organic photosensitizer featuring orderly conjugated ethylenedioxythiophene and dithienosilole blocks. *Chem Mater* 2010;22(5):1915–25.
- [19] Choi H, Raabe I, Kim D, Teocoli F, Kim C, Song K, et al. High mole extinction coefficient organic sensitizers for efficient dye-sensitized solar cells. *Chem Eur J* 2010;16(4):1193–201.
- [20] Yella A, Lee HW, Tsao HN, Yi C, Chandiran AK, Nazeeruddin MK, et al. Porphyrin-sensitized solar cells with cobalt(II/III)-based redox electrolyte exceed 12 percent efficiency. *Science* 2011;334:629.
- [21] Gao F, Wang Y, Zhang J, Shi D, Wang M, Humphry-Baker R, et al. A new heteroleptic ruthenium sensitizer enhances the absorptivity of mesoporous titania film for a high efficiency dye-sensitized solar cell. *Chem Commun* 2008:2635–7.
- [22] Yum JH, Jung I, Baik C, Ko J, Nazeeruddin MK, Grätzel M. High efficient donor-acceptor ruthenium complex for dye-sensitized solar cell applications. *Energy Environ Sci* 2009;2:100.
- [23] Kim M-J, Yu Y-J, Kim J-H, Jung Y-S, Kay K-Y, Ko S-B, et al. Tuning of spacer groups in organic dyes for efficient inhibition of charge recombination in dye-sensitized solar cells. *Dyes Pigment* 2012;95(1):134–41.
- [24] Jia J, Zhang Y, Xue P, Zhang P, Zhao X, Liu B, et al. Synthesis of dendritic triphenylamine derivatives for dye-sensitized solar cells. *Dyes Pigment* 2013;96:407–13.
- [25] Kitamura T, Ikeda M, Shigaki K, Inoue T, Anderson NA, Ai X, et al. Phenyl-conjugated oligoene sensitizers for TiO₂ solar cells. *Chem Mater* 2004;16:1806–12.
- [26] Hagberg DP, Yum J-H, Lee H, De Angelis F, Marinado T, Karlsson KM, et al. Molecular engineering of organic sensitizers for dye-sensitized solar cell applications. *J Am Chem Soc* 2008;130:6259–66.
- [27] Zhang F, Luo Y-H, Song J-S, Cuo X-Z, Liu W-L, Ma C-P, et al. Triphenylamine-based dyes for dye-sensitized solar cells. *Dyes Pigment* 2009;81:224–30.
- [28] Ko S-B, Cho A-N, Kim M-J, Lee C-R, Park N-G. Alkyloxy substituted organic dyes for high voltage dye-sensitized solar cell: effect of alkyloxy chain length on open-circuit voltage. *Dyes Pigment* 2012;94:88–98.
- [29] Hara K, Sato T, Katoh R, Furube A, Ohga Y, Shinpo A, et al. Molecular design of coumarin dyes for efficient dye-sensitized solar cells. *J Phys Chem B* 2003;107:597–606.
- [30] Hara K, Wang Z-S, Sato T, Furube A, Katoh R, Sugihara H, et al. Oligothiophene-containing coumarin dyes for efficient dye-sensitized solar cells. *J Phys Chem B* 2005;109:15476–82.
- [31] Kim S, Lee JK, Kang SO, Ko J, Yum J-H, Fantacci S, et al. Molecular engineering of organic sensitizers for solar cell applications. *J Am Chem Soc* 2006;128(51):16701–7.
- [32] Liu B, Zhu WH, Zhang Q, Wu WJ, Xu M, Ning ZJ, et al. Conveniently synthesized isophorone dyes for high efficiency dye-sensitized solar cells: tuning photovoltaic performance by structural modification of donor group in donor-acceptor system. *Chem Commun* 2009:1766–8.
- [33] Kim D, Song K, Kang M-S, Lee J-W, Kang SO, Ko J. Efficient organic sensitizers containing benzoc[d]indole: effect of molecular isomerization for photovoltaic properties. *J Photochem Photobiol A* 2009;201:102–10.
- [34] Matsui M, Ito A, Kotani M, Kubota Y, Funabiki K, Jin J, et al. The use of indoline dyes in a zinc oxide dye-sensitized solar cell. *Dyes Pigment* 2009;80:233–8.
- [35] Kim C, Choi H, Kim S, Baik C, Song K, Kang M-S, et al. Molecular engineering of organic sensitizers containing p-phenylene vinylene unit for dye-sensitized solar cells. *J Org Chem* 2008;73:7072–9.
- [36] Ning Z, Fu Y, Tian H. Improvement of dye-sensitized solar cells: what we know and what we need to know. *Energy Environ Sci* 2010;3(9):1170.
- [37] O'Regan BC, Durrant JR. Kinetic and energetic paradigms for dye-sensitized solar cells: moving from the ideal to the real. *Acc Chem Res* 2009;42:1799–808.
- [38] Boschloo G, Hagfeldt A. Characteristics of the iodide/triiodide redox mediator in dye-sensitized solar cells. *Acc Chem Res* 2009;42(11):1819–26.
- [39] Hamann TW, Jensen RA, Martinson ABF, Van Ryswyk H, Hupp JT. Advancing beyond current generation dye-sensitized solar cells. *Energy Environ Sci* 2008;1:66–78.
- [40] Nissfolk J, Fredin K, Hagfeldt A, Boschloo G. Recombination and transport processes in dye-sensitized solar cells investigated under working conditions. *J Phys Chem B* 2006;110(36):17715–8.
- [41] Robertson N. Optimizing dyes for dye-sensitized solar cells. *Angew Chem Int Ed Engl* 2006;45(15):2338–45.
- [42] Boschloo G, Häggman L, Hagfeldt A. Quantification of the effect of 4-tert-butylpyridine addition to I⁻/I₃⁻ redox electrolytes in dye-sensitized nanostructured TiO₂ solar cells. *J Phys Chem B* 2006;110(26):13144–50.
- [43] Wang P, Zakeeruddin SM, Humphry-Baker R, Moser JE, Grätzel M. Molecular-scale interface engineering of TiO₂ nanocrystals: improve the efficiency and stability of dye-sensitized solar cells. *Adv Mater* 2003;15(24):2101–4.
- [44] Snaith HJ, Schmidt-Mende L. Advances in liquid-electrolyte and solid-state dye-sensitized solar cells. *Adv Mater* 2007;19(20):3187–200.
- [45] Lee W, Cho N, Kwon J, Ko J, Hong JI. New organic dye based on a 3,6-disubstituted carbazole donor for efficient dye-sensitized solar cells. *Chem Asian J* 2012;7(2):343–50.
- [46] Wu Q-P, Xu Y-J, Cheng X-B, Liang M, Sun Z, Xue S. Synthesis of triarylamines with secondary electron-donating groups for dye-sensitized solar cells. *Sol Energy* 2012;86(2):764–70.
- [47] Ning ZJ, Zhang Q, Wu WJ, Pei HC, Liu B, Tian H. Starburst triarylamine based dyes for efficient dye-sensitized solar cells. *J Org Chem* 2008;73:3791.
- [48] Tang J, Hua JL, Wu WJ, Li J, Jin ZG, Long YT, et al. New starburst sensitizer with carbazole antennas for efficient and stable dye-sensitized solar cells. *Energy Environ Sci* 2010;3:1736–45.
- [49] Hagberg DP, Jiang X, Gabriëlsson E, Linder M, Marinado T, Brinck T, et al. Symmetric and unsymmetric donor functionalization. comparing structural and spectral benefits of chromophores for dye-sensitized solar cells. *J Mater Chem* 2009;19(39):7232.
- [50] Heo J, Oh J-W, Ahn H-I, Lee S-B, Cho S-E, Kim M-R, et al. Synthesis and characterization of triphenylamine-based organic dyes for dye-sensitized solar cells. *Synth Met* 2010;160(19–20):2143–50.
- [51] Lei BX, Fang WJ, Hou YF, Liao JY, Kuang DB, Su CY. All solid state electrolytes consisting of ionic liquid and carbon black for efficient dye-sensitized solar cells. *J Photochem Photobiol A* 2010;216:8–14.
- [52] Chen CJ, Liao JY, Chi ZJ, Xu BJ, Zhang XQ, Kuang DB, et al. Metal-free organic dyes derived from triphenylethylene for dye-sensitized solar cells: tuning of performance by phenothiazine and carbazole. *J Mater Chem* 2012;22:8994–9005.
- [53] Wu W, Zhang J, Yang H, Jin B, Hu Y, Hua J, et al. Narrowing band gap of platinum acetylidene dye-sensitized solar cell sensitizers with thiophene π -bridges. *J Mater Chem* 2012;22(12):5382.
- [54] Nazeeruddin MK, Pechy P, Renouard T, Zakeeruddin SM, Humphry-Baker R, Comte P, et al. Engineering of efficient panchromatic sensitizers for nanocrystalline TiO₂-based solar cells. *J Am Chem Soc* 2001;123(8):1613–24.
- [55] Wang Z, Sugihara H. N₃-sensitized TiO₂ films: in situ proton exchange toward open-circuit photovoltage enhancement. *Langmuir* 2006;22(23):9718–22.
- [56] Guo M, Diao P, Ren Y-J, Meng F, Tian H, Cai S-M. Photoelectrochemical studies of nanocrystalline TiO₂ co-sensitized by novel cyanine dyes. *Sol Energy Mater Sol Cells* 2005;88:23–35.
- [57] Karlsson KM, Jiang X, Eriksson SK, Gabriëlsson E, Rensmo H, Hagfeldt A, et al. Phenoxazine dyes for dye-sensitized solar cells: relationship between molecular structure and electron lifetime. *Chem Eur J* 2011;17:6415.
- [58] Yang J, Guo F, Hua J, Li X, Wu W, Qu Y, et al. Efficient and stable organic DSSC sensitizers bearing quinacridone and furan moieties as a planar π -spacer. *J Mater Chem* 2012;22(46):24356.
- [59] Thomas KRJ, Hsu YC, Lin JT, Lee KM, Ho KC, Lai CH, et al. 2,3-Disubstituted thiophene-based organic dyes for solar cells. *Chem Mater* 2008;20(5):1830–40.
- [60] Shen P, Tang Y, Jiang S, Chen H, Zheng X, Wang X, et al. Efficient triphenylamine-based dyes featuring dual-role carbazole, fluorene and spirofluorene moieties. *Org Electron* 2011;12(1):125–35.
- [61] Longo C, Nogueira AF, Paoli M-AdE, Cachet H. Solid-state and flexible dye-sensitized TiO₂ solar cells: a study by electrochemical impedance spectroscopy. *J Phys Chem B* 2002;106(23):5925–30.
- [62] Kern R, Sastrawan R, Ferber J, Stangl R, Luther J. Modeling and interpretation of electrical impedance spectra of dye solar cells operated under open-circuit conditions. *Electrochim Acta* 2002;47:4213–25.
- [63] Fabregat SF, Bisquert J, Garcia BG, Boschloo G, Hagfeldt A. Influence of electrolyte in transport and recombination in dye-sensitized solar cells studied by impedance spectroscopy. *Sol Energy Mater Sol Cells* 2005;87:117–31.
- [64] Xu MF, Li RZ, Pootrakulchote N, Shi D, Guo J, Yi ZH, et al. Tuning the energy levels of organic sensitizers for high-performance dye-sensitized solar cells. *J Phys Chem C* 2009;113(7):2966–73.